ResearchGate

See discussions, stats, and author profiles for this publication at: https://www.researchgate.net/publication/270703333

Dynamical bending analysis and optimization design for functionally graded thickness (FGT) tube

Article *in* International Journal of Impact Engineering · April 2015

DOI: 10.1016/j.ijimpeng.2014.12.007

CITATIONS
85

READS
730

6 authors, including:

Guangyong Sun
Hunan University
257 PUBLICATIONS **16,517** CITATIONS
SEE PROFILE

Xuanyi Tian
Hunan University
4 PUBLICATIONS **215** CITATIONS
SEE PROFILE

Jianguang Fang
University of Technology Sydney
127 PUBLICATIONS **6,115** CITATIONS
SEE PROFILE

Fengxiang Xu
Wuhan University of Technology
44 PUBLICATIONS **1,747** CITATIONS
SEE PROFILE

All content following this page was uploaded by Guangyong Sun on 12 May 2021.

The user has requested enhancement of the downloaded file.

International Journal of Impact Engineering 78 (2015) 128–137

Contents lists available at ScienceDirect

International Journal of Impact Engineering

journal homepage: www.elsevier.com/locate/ijimpeng

Dynamical bending analysis and optimization design for functionally graded thickness (FGT) tube

Guangyong Sun [a], Xuanyi Tian [a], Jianguang Fang [b], Fengxiang Xu [a], Guangyao Li [a,*], Xiaodong Huang [a,c]

[a] State Key Laboratory of Advanced Design and Manufacturing for Vehicle Body, Hunan University, Changsha, Hunan 410082, China
[b] School of Automotive Studies, Tongji University, Shanghai 201804, China
[c] Centre for Innovative Structures and Materials, School of Civil, Environmental and Chemical Engineering, RMIT University, GPO Box 2476, Melbourne 3001, Australia

ARTICLE INFO

Article history:
Received 11 July 2014
Received in revised form
17 November 2014
Accepted 19 December 2014
Available online 26 December 2014

Keywords:
Crashworthiness design
Multiobjective optimization
Functionally graded thickness
Thin-walled structures
Energy absorption

ABSTRACT

As a relatively new component with a higher efficiency of material utilization, functionally graded thickness (FGT) structure with desired varying wall thickness has been becoming more and more attractive. In order to sufficiently understand the crashworthiness of FGT under lateral impact, firstly, the finite element (FE) models of thin-walled columns with uniform thickness (UT) and FGT under lateral loading are established and validated by experimental results. It is exhibited that the FE simulations are in good agreement with experimental tests. Then, the crashworthiness of UT tube and the corresponding FGT tube is compared, and the results reveal that the FGT tube can absorb more energy but generate larger force than UT tube under the same weight. Further, parametric analyses show the gradient exponent, wall thickness range, the tube diameter and yielding stress have significant effects on the crashworthiness of FGT tubes. Finally, a multiobjective particle swarm optimization (MOPSO) method is used to optimally seek for those design parameters, where surrogate modeling methods are adopted to formulate the specific energy absorption (SEA) and peak crushing force functions. The results yielded from the optimization demonstrate that the FGT tube is superior to its uniform thickness counterpart in overall crashing behavior under lateral impact. Therefore, FGT tubes are recommended as potential absorbers of crashing energy under lateral loading.

© 2014 Elsevier Ltd. All rights reserved.

1. Introduction

Thin walled structures have the advantages of light weight, low price, high strength and stiffness, high reliability, excellent loading-carrying efficiency and energy absorption capacity, which have been widely used as energy absorbers in crashworthiness applications such as automobile, train and aeronautical industries to protect passenger from severe injury [1–3]. To better understand crashing mechanism of thin-walled structures and further improve the design quality of energy absorbers, exhaustive studies have been conducted by using analytical, numerical and experimental approaches for thin-walled structures with various sections, such as circular [4], square [5], hexagonal [6,7], top-hat [8], multi-cell [9,10], convex polygon [11], concave polygon [12], etc. Wierzbicki and Abramowicz [13], Abramowicz and Jones [14,15] derived some approximate theoretical formula based on the balance of external and internal work to predict the average crushing force of circular and square tubes under either statically or dynamically loading. The general characteristics of force–displacement curves for circular tubes and square tubes are similar: the axial force first reaches an initial peak, followed by a drop and then fluctuates. However, their collapse modes are very different. The concertina mode, diamond mode, mixed mode and global bucking are the main collapse modes for a circular tube, while the common collapse mode of square tubes are symmetric mode, asymmetric mode, extensional mode and global bucking [16]. These different collapse modes directly affect the energy absorption ability of thin-walled columns. Further, these theoretical models were validated experimentally by Langseth and Hopperstad [17], and Abramowicz and Jones [14]. Although these theoretical formula show good agreements with the experimental results for some simple thin-walled structures, it is still a difficult task to derive a closed-form formula to predict the

* Corresponding author. Tel.: +86 731 8881 1717; fax: +86 731 8882 2051.
E-mail address: gyli@hnu.edu.cn (G. Li).

http://dx.doi.org/10.1016/j.ijimpeng.2014.12.007
0734-743X/© 2014 Elsevier Ltd. All rights reserved.

crashworthiness responses for some complex thin-walled structures up to date. Fortunately, Non-linear explicit finite element (FE) codes such as PAM-CRASH, ABAQUS Explicit and LS-DYNA provide powerful tools available in numerical simulations of highly nonlinear dynamic response of complicate thin-walled structures, which have been successfully applied in the crashworthiness design of thin-walled structures [18–23].

The studies mentioned above mainly focused on the crashing behavior and energy absorption characteristics of thin-walled tubes under axial loading. In fact, the front, rear and side components of cars often collapse in bending mode, thus bending collapse should be considered when designing vehicle body [24–27]. In addition, a crash test study on 81 vehicles showed that up to 90% involved structural members failed in bending collapse mode [28]. Thus, it has a great significance to carry out the investigation into the bending behavior of thin-walled structures. The first comprehensive experimental and theoretical study on the bending performance of square and rectangular prismatic beams was made by Kecman [29]. He proposed simple failure mechanisms involving stationary and moving plastic hinge lines, and found the moment-rotation characteristics in the post-buckling range up to 40°. The proposed theory has been verified by quasi-static bending tests. Wierzbicki et al. [24] extended the concept of a superfolding element and derived a closed-form formula for the bending resistance of thin-walled box-section beams. Lately, Kim and Reid [25] proposed a more accurate theoretical solution to predict the bending collapse of thin-walled structures based on some existing analytical relationship [24]. Liu and Day [30] analyzed the bending collapse of the thin-walled channel section beams and derived their approximation moment-rotation characteristics. An empirical formula based on dimensional analysis has also been presented by Huang and Lu [31].

Generally, the bending collapse of thin-walled beams is localized in a plastic hinge, with the remaining parts of beams rotating as rigid bodies. Since the inward fold of plastic hinge significantly reduces the cross-section area of the crush zone, the plastic bending resistance drops significantly after local sectional collapse occurs at relatively small rotation angle [32]. A distinctive characteristic of such a deformation mechanism is that the plastic deformation is concentrated over a relatively narrow zone, which results in low energy absorption efficiency [27]. In order to achieve higher bending resistance and weight efficiency in energy absorption, ultra-light metal fillers such aluminum foams as honeycomb introduced into the thin-walled structures has attracted increasing interest. Santosa and Wierzbicki [33] and Santosa et al. [34] studied the effect of foam filling on the bending resistance of thin-walled prismatic columns through numerical simulations and quasi-static experiments. It was shown that filling of foam could improve the load-carrying capacity by offering additional support from inside and increased the absorbed energy, and concluded that partial filling of foam might be achieve even higher energy absorption to weight ratio of the structure. Chen et al. [35] carried out the numerical and experimental studies on the bending collapse of thin-walled tubes filled with aluminum foam or aluminum honeycomb. They showed the potentials of significant weight saving and volume reduction by utilizing ultralight metal filler. Zarei and Kroger [32] performed crashworthiness optimization for maximizing specific energy absorption on foam-filled tubes under bending, and found that the foam-filled tubes can save more weight to absorb the same energy. Recently, Yu and his co-authors [4,36,37] have carried out systematic experimental and numerical investigation into the performance of different topological thin-walled structures under three-point bending. Reyes et al. [38] developed a material model including fracture criteria for both extrusion and foam to study the influence of material failure on bending behavior of square aluminum extrusions filled with aluminum foam. Fang et al. [39] investigated and optimized the crashing behaviors of three types of functionally graded foam (FGF)-filled thin-walled structures subjected to lateral impact, and found that the FGF-filled tubes can provide better designs than the ordinary uniform foam (UF) filled counterpart.

Although the foam-filled thin-walled structures significantly improve the crashworthiness, the inherent discontinuity inside the metallic foam easily results in fracture at tensile flanges and diminishes the energy absorption [38,40], which directly limits the application of foam-filled thin-walled structures under bending load to some extent. In addition, the traditional thin-walled tube always form a localized plastic hinge on the compressed flanges for bending collapse, which weakens the impact resistant force and reduces the energy absorption. Therefore, some new thin-walled structures without foam filler need to be developed. In brief, if we can prevent or delay the formation of the localized plastic hinge, the bending collapse of thin-walled columns could be significantly improved. Based on this principle, a novel thin-walled structure named functionally graded thickness (FGT) tube will be presented in this paper. Unlike existing thin-walled structures with uniform thickness, the wall thickness of the present FGT tube varies along the longitudinal direction with a certain gradient. To the authors' best knowledge, no study has been conducted on the energy absorption response of non-uniform thickness thin-walled structures under lateral loads so far. Although fabricating FGT structures could be inherently more sophisticated than making uniform thickness (UT) structures, some advanced technologies e.g. tailor rolling blanks have been available to produce such structures with a given gradient [41,42]. It is the time to make use of FGT tubes for energy absorption under impact scenarios. To do so, it is essential to understand the energy absorption characteristics in comparison with those well-studied uniform thickness (UT) thin-walled structures under lateral loading. On the other hand, crashworthiness design of thin-walled structures is typically characterized by a number of quality and/or performance indices such as peak crushing force, specific energy absorption (SEA) and crash load efficiency, some of which could conflict with each other. Therefore, it is of particular significance to seek the best possible thickness gradient for optimal crashworthiness under multiple criteria.

In this paper, the energy absorption characteristic of FGT tube under lateral impact loading is studied by using nonlinear element code LS-DYNA. After validating finite element model with experiments, the effects of various parameters including the gradient exponent, wall thickness range, the tube diameter and yielding stress on the crashworthiness of FGT tubes are analyzed. Finally, a multiobjective particle swarm optimization method [43] is used to optimize those parameters, where surrogate modeling methods are adopted to formulate the specific energy absorption (SEA) and peak crushing force functions. To efficiently approximate the responses of interest, several widely-used surrogate modeling techniques such as Kriging, response surface method (RSM) and radial basis function (RBF) are compared with each other. The results will demonstrate that the FGT tube provides better crashworthiness performance than the UT tube.

2. Simulation modeling and experimental validation

2.1. Structural crashworthiness indicators

In order to evaluate the crashworthiness of the thin-walled structures under lateral impact load, peak crash force (F_{max}), energy absorption (EA), specific energy absorption (SEA) and crash force efficiency (CFE) are usually used as the important indicators for evaluating the crashworthiness.

The energy absorption of a structure subjected to the lateral impact load can be expressed as

$$EA(d) = \int_0^d F(x)dx \tag{1}$$

where d is a given deformation distance and $F(x)$ denotes the corresponding crushing force. The specific energy absorption is defined as the ratio of the absorbed energy to the mass of the structure and can be written as [44].

$$SEA(d) = \frac{EA(d)}{M} \tag{2}$$

where M is the total mass of the structure. Apparently, the higher the SEA, the better the energy absorption capacity of a structure. Another indictor in relation to energy absorption capacity is crash force efficiency (CFE), which can be given as [45].

$$CFE = \frac{F_{avg}}{F_{\max}} \times 100\% \tag{3}$$

where $F_{\max}$ is the maximum impact force during the whole collision progress. F_{avg} is the mean crash force expressed as the total energy absorption divided by the corresponding crushing displacement, as

$$F_{avg} = \frac{EA(d)}{d} \tag{4}$$

2.2. Functional graded column

Fig. 1 illustrates the key geometrical features of the circular column under lateral impacting loads. The column lays on two cylindrical supports, and the span and diameters are 230 mm and 46 mm, respectively. A cylindrical punch with a diameter of 10 mm and a mass of 14.44 kg impacts on the mid-span of columns and an initial velocity of $v_0 = 3.44$ m/s. As the local deformation zone is in the middle, it is reasonable that the middle thickness is set as the maximum value $t_{\max}$ and both ends as minimum $t_{\min}$. The corresponding profile is shown in Fig. 1(b). It is assumed that the circular column is fabricated with gradually varying wall thickness along the axial direction. The idea is similar to the density gradient of the functionally graded foam materials developed by authors [3]. In the axial gradient case (x-direction), the thickness variation $t_f(x)$ can be defined through the following power law function:

$$t_f(x) = t_{\min} + (t_{\max} - t_{\min})\left(\frac{2x}{L}\right)^m \tag{5}$$

where x is the distance starting from the left end to punch location ($0 \le x \le L/2$ due to symmetric), and m is the gradient exponent and assumed to vary between 0 and 10 in this study. L represents the total length of the column. From Eq. (5), it is easily found that the wall thickness increases along the length with a gradient function changing from convexity to concavity correspondingly when the gradient exponent m value varies from less than 1 to greater than 1, as shown in Fig. 2.

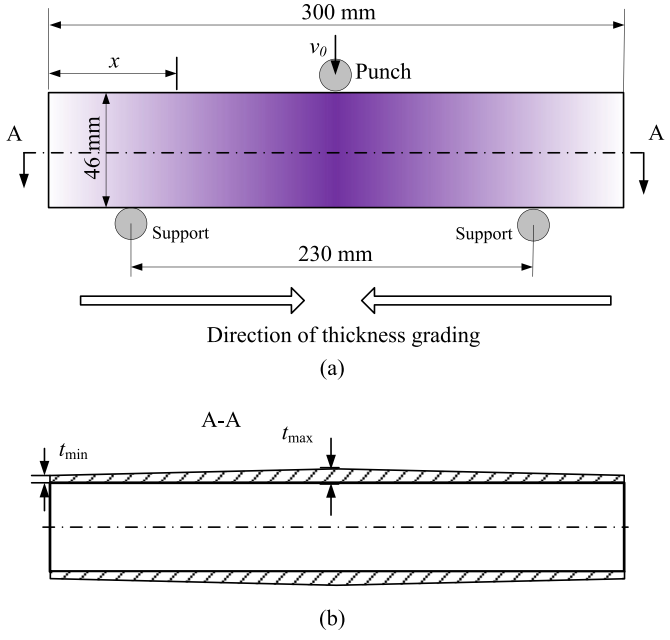

Fig. 1. Schematic and profile showing thickness grading patterns in the axial direction: (a) Front view; (b) A–A cross-sectional view.

2.3. Numerical models and validation

2.3.1. Finite element modeling

The numerical models are developed using explicit non-linear finite element code LS-DYNA in this study. Fig. 3 shows the finite element model subjected to lateral impact. Belytschko-Tsay reduced integration shell elements with five integration points through the shell thickness were employed to model the wall of column, support and punch. Compared with column, the support and punch are almost not deformation, thus they are taken as rigid body. Stiffness-based hourglass control was employed to avoid spurious zero energy deformation modes, and reduced integration was used to avoid volumetric locking. The contact between the punch and the tube column is modeled with a surface-to-surface contact algorithm with a friction coefficient of 0.3. The contact between the supports and the specimen is also simulated with a surface-to-surface contact with the friction coefficient of 0 in order to allow sliding rotation [27]. The "automatic single surface" contact was used to prescribe the column wall itself to avoid interpenetration of column folding during bending collapse.

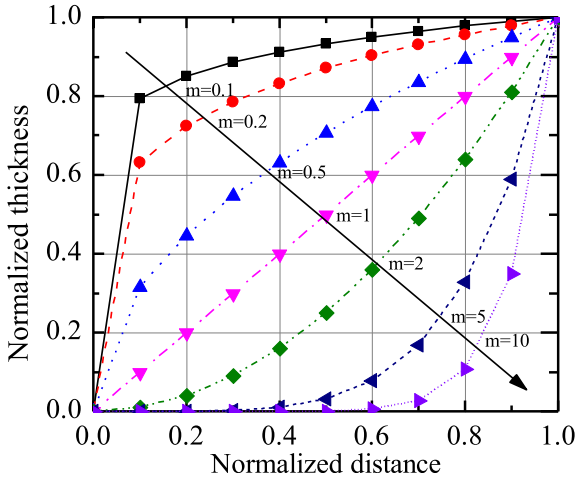

Fig. 2. Variation of normalized thickness (0 = $t_{\min}$, 1 = $t_{\max}$) *vs* normalized distance (0 = left/right cross-section, 1 = middle cross-section).

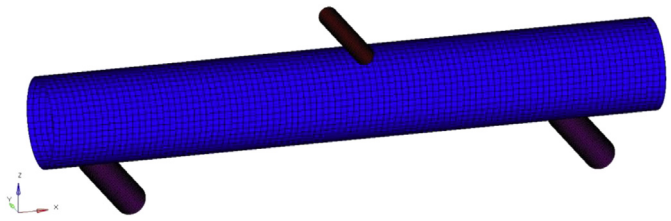

Fig. 3. Finite element model.

The material of thin wall column considered herein is aluminum alloy AA6061. The engineering stress–strain curve which is obtained by the standard uniaxial tension test depicted in Fig. 4. The mechanical properties are as follow: density $\rho = 2700$ kg/m^3, Poisson's ratio $\nu = 0.3$, Young's modulus $E = 70$ GPa. The constitutive behavior of the aluminum column was modeled via the piecewise linear plasticity material model, Mat 24, in LS-DYNA [46]. The strain rate effect was neglected as the aluminum alloy is strain rate insensitive material [17].

For an ideal continuous variable thickness tube, the column wall should be divided to an infinite number of layers to approximate the actual thickness variation. In the finite element framework, the minimum width of a layer would be equal to the size of each shell element. In order to determine the optimum element size to balance the accuracy and computational cost, a convergence test with five different mesh sizes was carried out. The convergence results are listed in Fig. 5. From which, it can be found that the relative error between element sizes 2 mm and 3 mm is less than 1% for both FGT and UT. Further element refinement will not improve the accuracy significantly, while the computational efficiency will be largely decreased. Therefore, the optimum element size is 3 mm × 3 mm, which is adopted throughout this paper.

2.3.2. Validation of the numerical model

To evaluate the effectiveness of the simulation models of FGT and UT tubes, the UT tube with the 1.5 mm thickness and the FGT tube with $t_{max} = 1.5$ mm, $t_{min} = 0.8$ mm and $m = 1$ were made and tested. The curves of force versus displacement and deformation of the experiments and simulations are given in Fig. 6. From which, it can be seen that the simulation results agree well with experimental results. The validation provides considerable confidence for us in exploring the energy absorption capacity of thin-walled

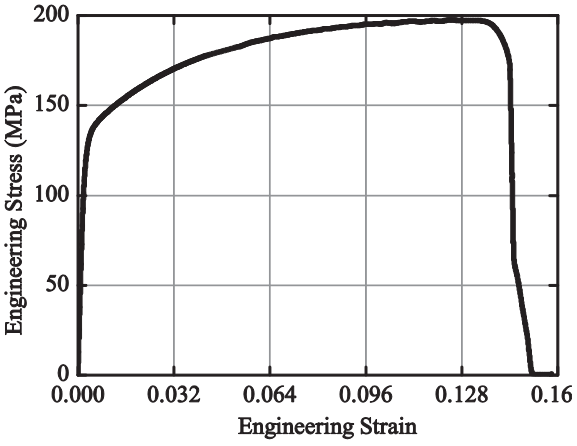

Fig. 4. Engineering stress–strain curves.

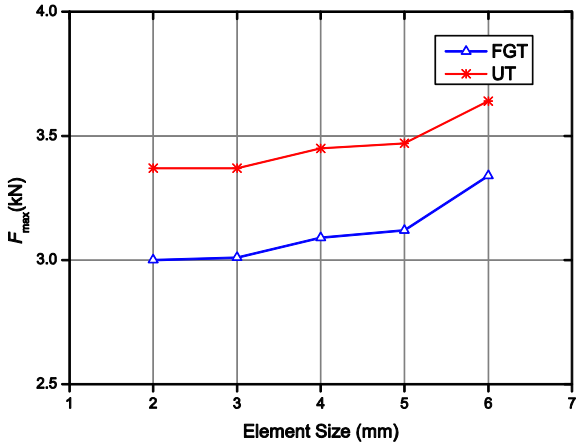

Fig. 5. Convergence results of element sizes.

circular column and optimization using the developed numerical model.

3. Parametric analyses

To better understand the crashworthiness characteristics of FGT tubes under lateral impact loading, it is necessary to carry out the comprehensive parametric analyses. In this section, the parametric analyses mainly investigate the effects of the gradient exponent parameter, thickness range, diameter and yield stress of the tubes on crashworthiness performance. Because the crashworthiness indicators are essentially related with the given deformation distance, for comparison, the deformation distance is set as 40 mm for all these following parametric analyses and optimization design.

3.1. Effect of thickness variation

In order to compare the energy absorption capacity between UT tubes and FGT tubes under the same weight, numerical simulations of the FGT tubes with different gradient parameters are performed. For all the FGT tubes, $t_{\max}$ and $t_{\min}$ are defined as 1.5 mm and 0.8 mm, respectively. To easily calculate the equivalent thickness (t_{avg}) of UT tube, it is assumed that the length of each layer is the same and defined as L_e. Thus the t_{avg} can be given as follows,

$$t_{avg} = \sum_{i=1}^{N}(t_i L_e)/(NL_e) = \sum_{i=1}^{N} t_i/N \tag{6}$$

where N denotes the total number of element layers of the FGT tube along the axial direction, and t_i is thickness of the ith layer element.

Fig. 7(a) and (b) compare the change trend of F_{max} and EA of the UT and FGT tubes with increasing gradient parameters, respectively. Generally, FGT tubes have larger values of $F_{\max}$ and EA comparing with their UT counterparts. Moreover, FGT tubes can produce larger SEA than UT tubes as shown in Fig. 7(c). It can also be found from Fig. 7(c) that the SEA of FGT tubes increases up to a peak value and then decreases with the increasing of the gradient exponent parameter m. Thus, the FGT tube seems much more promising than the corresponding UT tube in terms of EA and SEA. The reason mainly lies in that the thickness of FGT tube is highest at the region of severe deformation (mid-span part of the tube). Meanwhile, Fig. 7(d) shows the similar relationship between CFE and m of the FGT tube and the corresponding UT tube. Note that CFE of the FGT tube is only slightly bigger than that of the corresponding UT tube when $m < 4$.

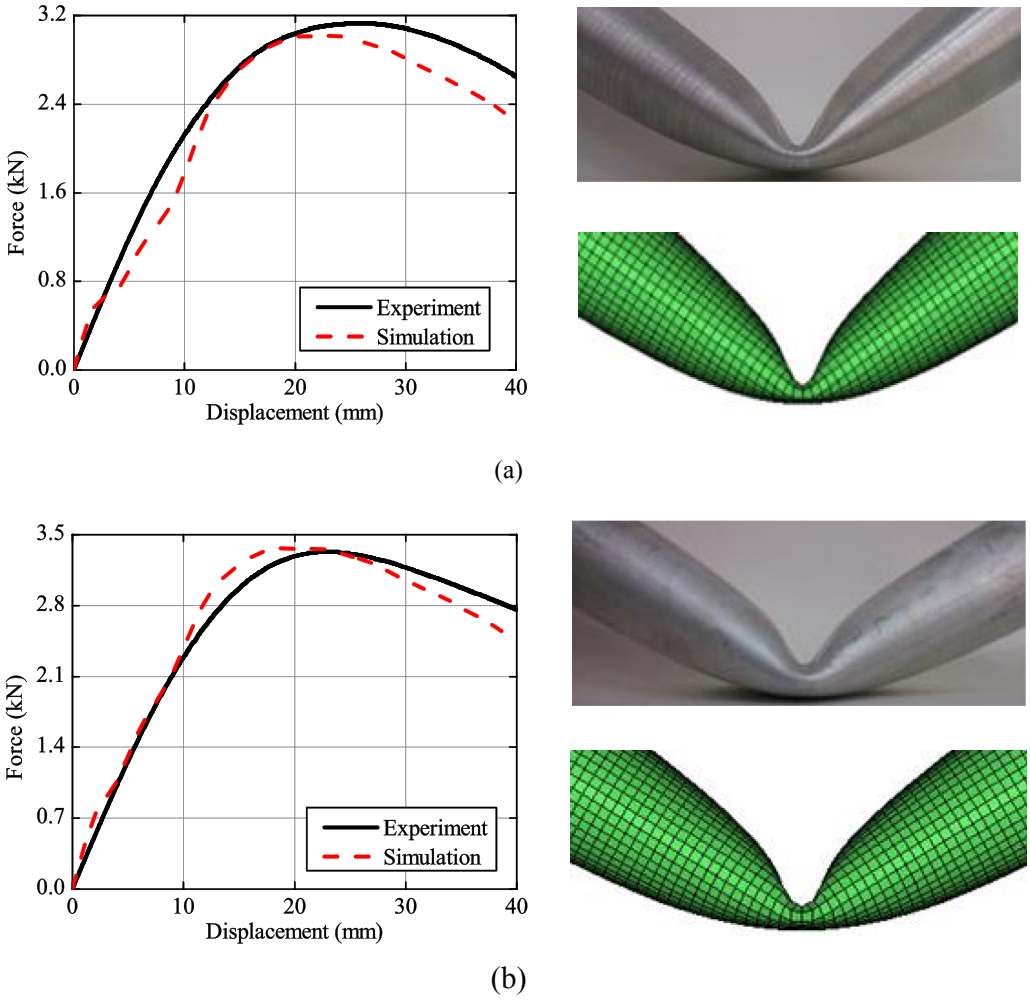

Fig. 6. Comparison between experiments and FE simulations (a) FGT tube (t_{max} = 1.5 mm, t_{min} = 0.8 mm and m = 1); (b) UT tube (t = 1.5 mm).

3.2. Effect of thickness range

To explore the effect of wall thickness range ($\Delta p = t_{\max} - t_{\min}$) on the crashworthiness of FGT tube, the value of $t_{\min}$ was varied with 0.8, 1.0 and 1.2 mm while the $t_{\max}$ = 1.5 mm. Fig. 8(a)-(c) display $F_{\max}$, *EA* and *SEA* of FGT tubes with different gradient exponent m. Note that the thickness range (Δp) has a noticeable effect on crashworthiness performance. Specifically, larger values of Δp (smaller values of $t_{\min}$) can help improving *SEA*, while it could have a negative effect on *EA*. Besides, it could also reduce the values of $F_{\max}$. Meanwhile, it can be found from Fig. 8(d) that the *CFE* is decreased with Δp increasing.

3.3. Effect of diameter

Four diameters of columns (d = 40 mm, 44 mm, 48 mm and 52 mm) are considered here. Fig. 9(a) and (b) give the $F_{\max,}$ and *EA* of four diameters of FGT tubes with different gradient exponent m. It can be found that $F_{\max,}$ and EA of four diameters are all decreased with the increasing of m. $F_{\max}$ of the FGT tube with a diameter of 40 mm is superior to others. Generally, the larger the diameter, the greater $F_{\max.}$ The rule of $F_{\max}$ is completely different with that of EA. EA of the FGT tube with a diameter 55 mm is better than other tubes for $0 \le m \le 0.8$. For $0.8 < m < 4$, the diameter of 48 mm shows the best EA performance. However, the energy absorption of tube with a diameter of 44 mm becomes the highest for $m \ge 4$. In addition, it can also be found from Fig. 9(a) and (b) that the differences of $F_{\max}$ and EA between four diameters shrink with the increasing of m, respectively.

Fig. 9(c) gives the tendency of SEA for different diameters with an increase of gradient exponent m. It can be seen that *SEA*s of FGT tubes increase up to their peak values and then decrease with the increasing of m. Meanwhile, SEA of the FGT tube with the diameter of 40 mm is larger than other tubes. From Fig. 9(d), it is observed that the difference of *CFE* is not so obvious with the change of diameters when $m < 1$, while the change of *CFE* is significant when $m \ge 1$. CFE is largest for the FGT tube with a diameter of 44 mm when $m < 2$, while the FGT with the 40 mm diameter is the best selection when $m \ge 2$.

3.4. Effect of yielding stress

Fig. 10(a)-(c) depict $F_{\max}$, *EA* and *SEA* of FGT tubes with different yielding stress (σ_y = 120, 135, 150 and 165 MPa). It shows that $F_{\max}$, *EA* and *SEA* will increase with the increasing of yielding stress for all gradient exponents m. However, it can be found from Fig. 10(d) that the *CFE* is decreased with the increasing of yielding stress. Because the variation of yielding stress does not change the column mass at each specific case of m, the *SEA* values of different yielding stress follow the same order of magnitude as the *EA* values. The only difference is that the *SEA* values first increase and then decrease while the *EA* values decrease monotonically with the increasing of m.

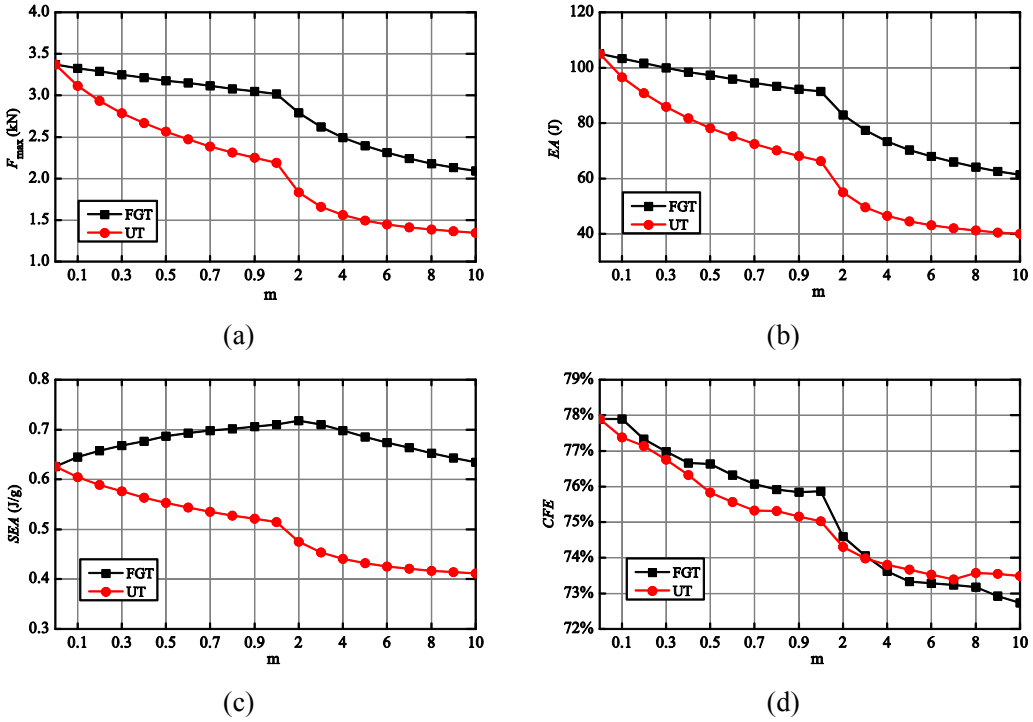

Fig. 7. Energy absorption characteristics versus gradient exponent m of the FGT tubes and the corresponding UT tubes: (a) F_{max}; (b) EA; (c) SEA; (d) CFE.

It can also be observed that the tubes with $\sigma_y = 165$ MPa and 120 MPa perform worst and best for F_{max} and *CFE*, respectively. Therefore, the columns with lower σ_y are preferred in terms of these two indicators. However, this conclusion conflicts with the requirements of *SEA* and *EA*, that is, the lower yield stress will result into the smaller *SEA* and *EA*.

4. Multiobjective optimization design

4.1. Multiobjective optimization problem

As an energy absorber, the column structure is expected to absorb as much energy as possible per unit mass. Thus, the *SEA*

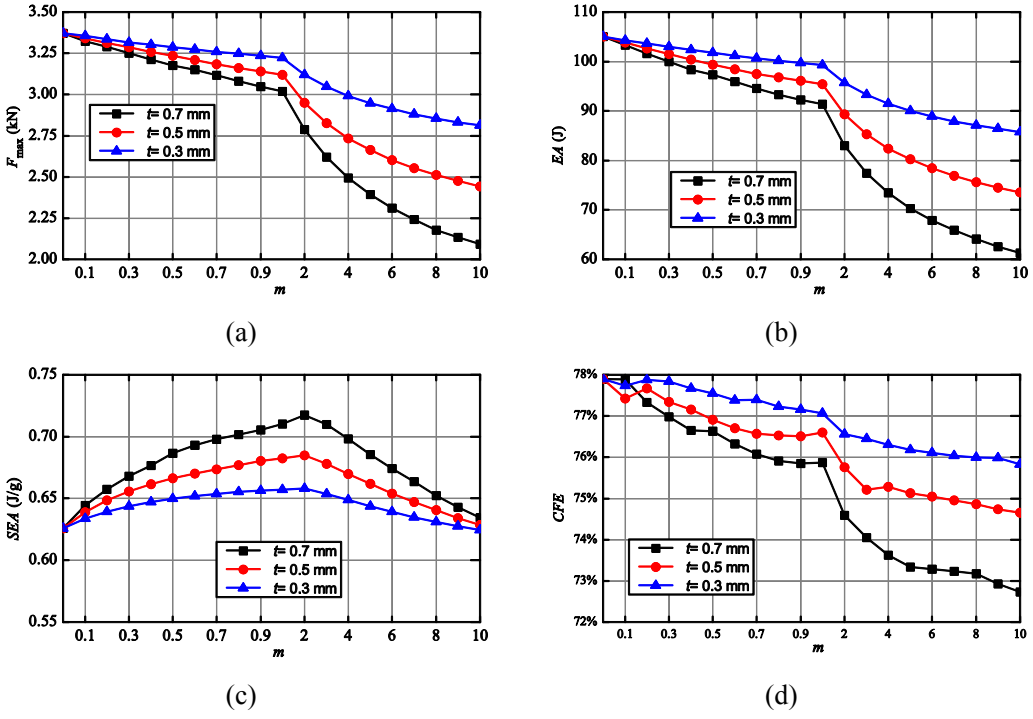

Fig. 8. Variation of crashworthiness performance vs thickness range: (a) F_{max}; (b) EA; (c) SEA; (d) CFE.

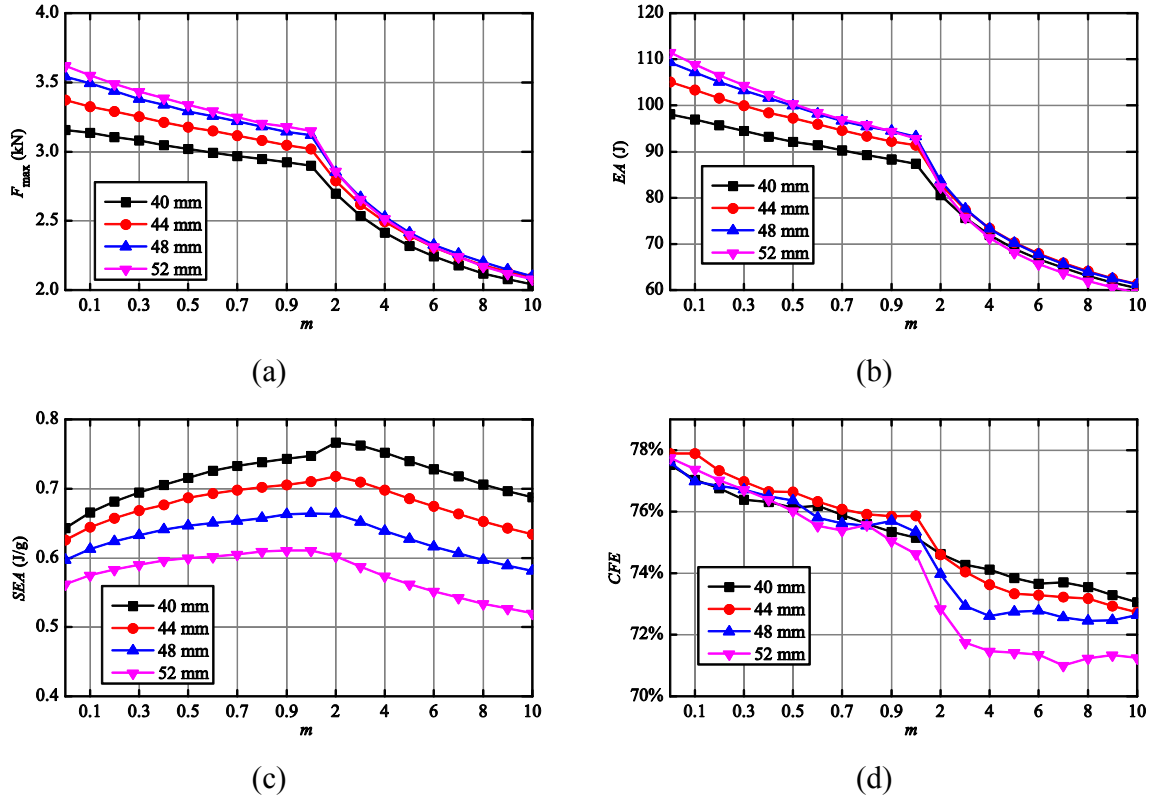

Fig. 9. Comparisons of energy absorption characteristics of FGT tube with different diameters: (a) F_{max}; (b) EA; (c) SEA; (d) CFE.

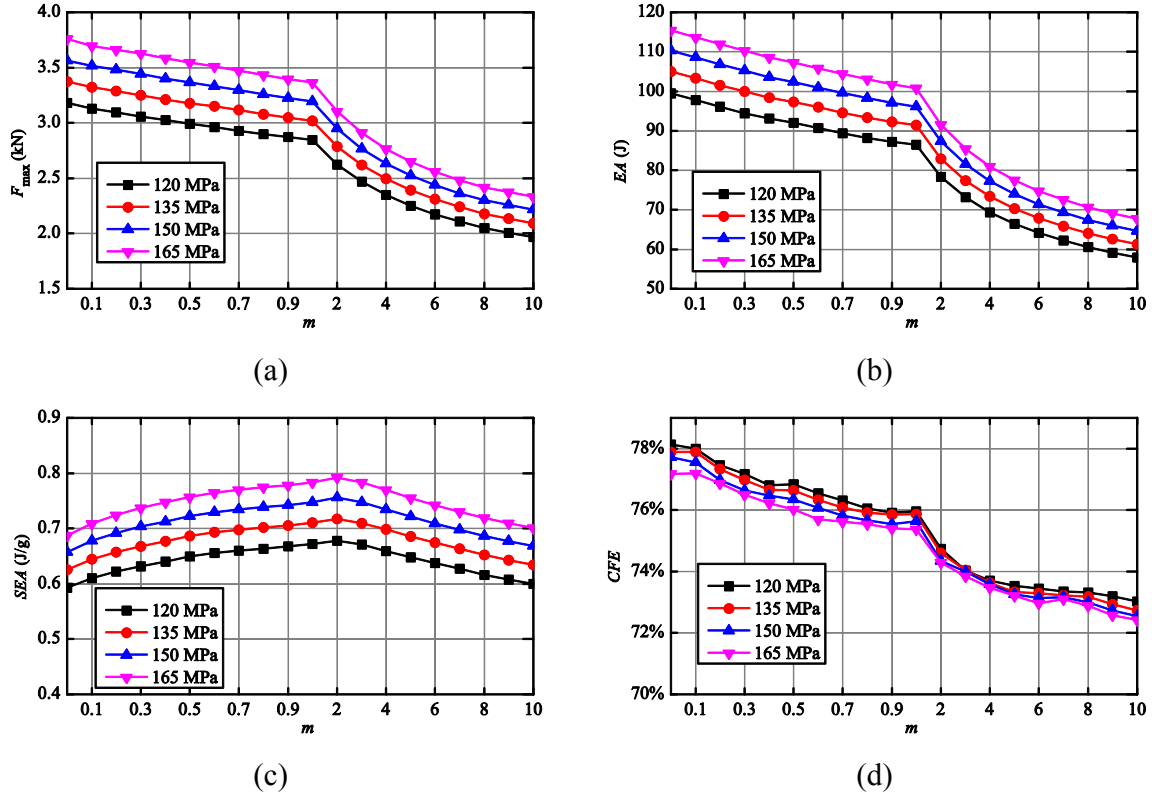

Fig. 10. Comparisons of energy absorption characteristics of FGT tube with different yielding stress: (a) F_{max}; (b) EA; (c) SEA; (d) CFE.

should be an objective function and maximized. Besides, $F_{\max}$ is another indicator for the safety of the occupants, which should be minimized. Therefore, the optimization problem can be formulated in a multiobjective framework as follows:

$$\begin{cases} Minimize & [F_{\max}(m,d,\sigma_y),\ -SEA(m,d,\sigma_y)] \\ Subject & to \begin{cases} m^L \le m \le m^U \\ d^L \le d \le d^U \\ \sigma_y^L \le \sigma_y \le \sigma_y^U \end{cases} \end{cases} \tag{7}$$

where m is the gradient exponent, d is the diameter, σ_y is the yielding stress of column wall, superscript L and U are lower limit and upper limit of parameter; m^{L} and m^{U} are 0 and 10, d^{L} and d^{U} are 40 mm and 52 mm, σ_y^L and σ_y^U are 120 MPa and 165 MPa, respectively.

4.2. Surrogate model and error metrics

It is difficult to derive analytical objective functions mathematically for SEA and $F_{\max}$ that involve highly nonlinear contact-impact and large deformation mechanics, such as crashworthiness [3]. As an alternative, surrogate model is an effective way to alternate mathematical formulation of the relation between the design variables and responses, which will also reduce the cost of computation. For different problems, the precision of different surrogate model are not the same. In this study, three different surrogate models, Kriging approximation model (KRG) [47], response surface method (RSM) [48] and radial basis function (RBF) [49], are considered. Among these surrogates, the most accurate surrogate will be picked up to perform the multiobjective optimization design. To construct high accuracy surrogate, design of experiment (DOE) often was used to sample the design space. Of many different DOE methods available, Latin hypercube sampling (LHS) is used to generate the training points in the design space [50]. To capture high nonlinear responses, 200 training points are generated in this study.

To assess the modeling accuracy of the RSM, KRG and RBF, 20 additional validation points are randomly generated. Three numerical estimators, namely R-square (R^2), Root-Mean-Square-Error (RMSE) and Maximum-Absolute-Percentage-Error (MAPE) are used to validate the accuracy of these surrogate models [51], as given in Eqs. (8)–(10).

$$R^2 = 1 - \frac{\sum_{i=1}^{M}(y_i - \hat{y}_i)^2}{\sum_{i=1}^{M}(y_i - \bar{y})^2} \tag{8}$$

$$RMSE = \sqrt{\frac{1}{M}\sum_{i=1}^{M}(\hat{y}_i - y_i)^2} \tag{9}$$

$$MAPE(\%) = \max\left(\left|\frac{\hat{y}_i - y_i}{y_i}\right|\right) \times 100(\%) \tag{10}$$

where M is the number of validation points, y_i is the true values, $\hat{y}_i$ is the corresponding approximate surrogate values, and $\bar{y}$ is the mean of y_i. These performance metrics reflect the prediction capability of the surrogate models at some new points to some extent. Generally, the R^2 and RMSE metrics indicate the overall accuracy of an approximation model, while the MAPE metrics indicate a local metrics, which describes the error in a sub-region of the design space. Overall, the closer the value of R^2 to unity and/or the smaller the values of RMSE and MAPE, the higher the accuracy.

4.3. Results and discussion

4.3.1. Accuracy of surrogate models

Tables 1 and 2 show the accuracy assessment of these surrogates for FGT and UT tubes, respectively. It can be seen that RBF and Quartic-RSM surrogates are the most accuracy surrogate model in the approximation of F_{max} for FGT tube and UT tube, respectively. But for the approximation of SEA, the Quartic-RSM surrogate model is the most accuracy surrogate for the FGT and UT tube. The most accurate surrogates will be used to solve the optimization problem.

4.3.2. Optimization results

To obtain the optimal design of the FGT and UT tubes, a multi-objective particle swarm optimization (MOPSO) is used herein. As an extension to the particle swarm optimization (PSO), MOPSO has drawn considerable attention recently because of its relatively fast convergence and well-distributed Pareto front [52]. The Pareto fronts of the FGT tubes and the corresponding UT tubes are shown in Fig. 11. It can be seen that the Pareto front of FGT is located in the lower left of that of UT, which indicates that the FGT has more excellent crashworthiness. Besides, it is clearly seen that *-SEA* and $F_{\max}$ are negatively correlated for FGT and UT tubes, which means that an increase of *SEA* (decrease of *-SEA*) always leads to an increase of $F_{\max}$ or decrease of $F_{\max}$ results in a reduction of *SEA*. These two performances can't attain simultaneously the optimal solution. Such problem is very fit to be solved by multiobjective optimization algorithm. By which, we can obtain a range of optimal solutions (Pareto front) in a single run, not just an optimal point. These solutions provide a large of design schemes for decision-maker. Here, the designers can effectively search for a more sophisticated optimal solution according to their design requirements.

Table 1
Accuracy assessment of the surrogate models for FGT tube.

Responses	Surrogate models		Estimators		
			R^2	RMSE	MAPE (%)
F_{max} (kN)	KRG	–	0.8627	0.1395	11.4548
	RBF	–	0.9991	0.0112	0.9271
	RSM	Linear	0.9110	0.1123	8.9026
		Quadratic	0.9911	0.0354	2.3664
		Cubic	0.9964	0.0226	1.8135
		Quartic	0.9966	0.0220	2.1162
SEA (J/g)	KRG	–	0.7140	0.0325	12.8440
	RBF	–	0.9899	0.0061	3.5530
	RSM	Linear	0.8223	0.0256	11.8580
		Quadratic	0.9308	0.0160	7.2242
		Cubic	0.9728	0.0100	4.3019
		Quartic	0.9837	0.0078	3.0405

Table 2
Accuracy assessment of the surrogate models for UT tube.

Responses	Surrogate models		Estimators		
			R^2	RMSE	MAPE (%)
F_{max} (kN)	KRG	–	0.5923	0.3095	30.6333
	RBF	–	0.9784	0.0712	8.8250
	RSM	Linear	0.7143	0.2591	23.0073
		Quadratic	0.9270	0.1309	12.9272
		Cubic	0.9846	0.0602	6.7023
		Quartic	0.9948	0.0348	3.3140
SEA (J/g)	KRG	–	0.5377	0.0465	22.2011
	RBF	–	0.9894	0.0071	4.2059
	RSM	Linear	0.8415	0.0272	11.3773
		Quadratic	0.9648	0.0128	6.1665
		Cubic	0.9940	0.0053	2.3621
		Quartic	0.9987	0.0024	1.1598

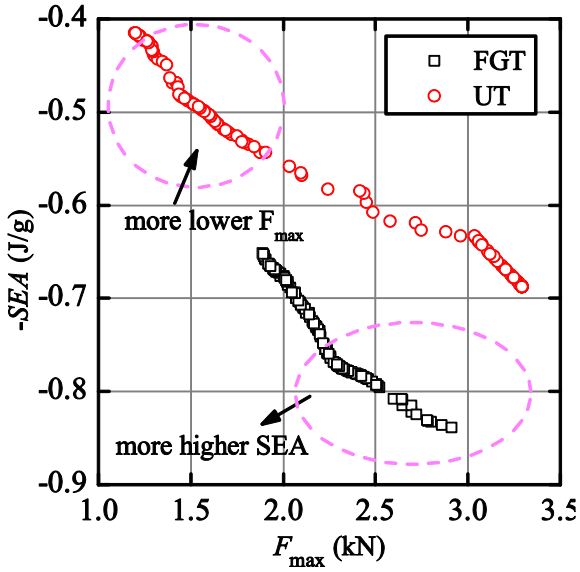

Fig. 11. Comparison of Pareto fronts of the FGT tube and UT tube.

The ideal optimal values of the two single objective functions *SEA* and F_{max} are provided in Table 3. Here, the "ideal" means only a single objective (*SEA* or F_{max}) is pursued. These four single "ideal" optimums listed in Table 3 correspond to the four special points in the Pareto space, which just lie at both ends of the Pareto curves. It can be seen from Table 3 that the FGT is superior to UT in Ideal Max *SEA* which is 0.83 J/g and 0.68 J/g, respectively. However, the Ideal Min F_{max} of FGT (1.88 kN) is worse than that of UT (1.19 kN). If we only aim to low F_{max}, we can adopt UT tube. Otherwise, we perfect to use the FGT tube.

5. Conclusions

In this paper, a functionally graded thickness (FGT) tube under lateral impact loads has been investigated by employing the validated finite element model. A series of FGT tubes whose gradient exponent varies from 0 to 10 are compared with the uniform thickness (UT) tubes under the same weight. It was found that the FGT tubes would provide better values in the specific energy absorption (*SEA*), energy absorption (*EA*) and crash force efficiency (*CFE*) but worse values in maximum impact force (F_{max}). Through the further parametric study, the gradient exponent, thickness range, diameter of tube and yielding stress of wall material could affect the crashworthiness performance significantly. To achieve the optimum design for the crashworthiness of UT and FGT tubes, the multiobjective optimization problems are formulated, aiming to simultaneously minimize the F_{max} and maximize the *SEA*. The optimal results show that the FGT and UT tubes have their cons and pros in practical applications. As the *SEA* is the most important indicator of an energy absorber for the designers, in this sense, FGT tubes can provide better crashworthiness performance than UT tubes under bending.

Table 3
Ideal optimums of the two single objective functions for the FGT and UT tubes under lateral impact.

Type	Single objective	m	d (mm)	σ_y(MPa)	SEA (J/g)	F_{max} (kN)
FGT	Ideal Max *SEA*	2.48	40	165	0.83	2.91
	Ideal Min F_{max}	10.00	40	120	0.65	1.88
UT	Ideal Max *SEA*	0.00	40	165	0.68	3.29
	Ideal Min F_{max}	8.51	40	120	0.41	1.19

Acknowledgment

This work was supported from The National Natural Science Foundation of China (11202072, 11102067), The Doctoral Fund of Ministry of Education of China (20120161120005), The Hunan Provincial Science Foundation of China (13JJ4036) and the Program of the Methodology Study on Designing Automotive Parts with Variable Thickness Blanks (QYT-KT-2013-003).

References

[1] Alghamdi. Collapsible impact energy absorbers: an overview. Thin Walled Struct 2001;39(2):189–213.
[2] Abramowicz W. Thin-walled structures as impact energy absorbers. Thin Walled Struct 2003;41(2–3):91–107.
[3] Sun GY, Li GY, Hou SJ, Zhou SW, Li W, Li Q. Crashworthiness design for functionally graded foam-filled thin-walled structures. Mater Sci Eng A 2010;527:1911–9.
[4] Li ZB, Zheng ZJ, Yu JL, Guo LW. Crashworthiness of foam-filled thin-walled circular tubes under dynamic bending. Mater Des 2013;52:1058–64.
[5] Yang S, Qi C. Multiobjective optimization for empty and foam-filled square columns under oblique impact loading. Int J Impact Eng 2013;54:177–91.
[6] Liu YC. Thin-walled curved hexagonal beams in crashes – FEA and design. Int J Crashworthiness 2010;15(2):151–9.
[7] Hou SJ, Li Q, Long SY, Yang XJ, Li W. Design optimization of regular hexagonal thin-walled columns with crashworthiness criteria. Finite Elem Analysis Des 2007;43(6–7):555–65.
[8] White MD, Jones N. Experimental study into the energy absorbing characteristics of top-hat and double-hat sections subjected to dynamic axial crushing. Proc Institution Mech Eng Part D J Automob Eng 1999;213(D3):259–78.
[9] Yin HF, Wen GL, Liu ZB, Qing QX. Crashworthiness optimization design for foam-filled multi-cell thin-walled structures. Thin Walled Struct 2014;75:8–17.
[10] Zhang X, Zhang H. Energy absorption of multi-cell stub columns under axial compression. Thin Walled Struct 2013;68:156–63.
[11] Mamalis AG, Manolakos DE, Loannidis MB, Kostazos PK, Dimitriou C. Finite element simulation of the axial collapse of metallic thin-walled tubes with octagonal cross-section. Thin Walled Struct 2003;41(10):891–900.
[12] Fan Z, Lu G, Liu K. Quasi-static axial compression of thin-walled tubes with different cross-sectional shapes. Eng Struct 2013;55:80–9.
[13] Wierzbicki T, Abramowicz W. On the crushing mechanics of thin-walled structures. J Appl Mech 1983;50(4a):727–34.
[14] Abramowicz W, Jones N. Dynamic axial crushing of square tubes. Int J Impact Eng 1984;2(2):179–208.
[15] Abramowicz W, Jones N. Dynamic progressive buckling of circular and square tubes. Dynamic progressive buckling of circular and square tubes. Int J Impact Eng 1986;4(4):243–70.
[16] Zhang X, Cheng GD, Zhang H. Theoretical prediction and numerical simulation of multi-cell square thin-walled structures. Thin Walled Struct 2006;44(11):1185–91.
[17] Langseth M, Hopperstad OS. Static and dynamic axial crushing of square thin-walled aluminium extrusions. Int J Impact Eng 1996;18(7–8):949–68.
[18] Zhou Q, Wu XY, Xia Y, Cai WN. Spot weld layout optimization of tube crash performance with manufacturing constraints. J Manuf Sci Eng Trans ASME 2014;136(1):011014.
[19] Trimino LF, Cronin DS. Non-direct similitude technique applied to the dynamic axial impact of bonded crush tubes. Int J Impact Eng 2014;64:39–52.
[20] Qureshi OM, Bertocchi E. Crash performance of notch triggers and variable frequency progressive-triggers on patterned box beams during axial impacts. Thin Walled Struct 2013;63:98–105.
[21] Ghamarian A, Zarei HR, Abadi MT. Experimental and numerical crashworthiness investigation of empty and foam-filled end-capped conical tubes. Thin Walled Struct 2011;49(10):1312–9.
[22] Yin HF, Wen GL, Hou SJ, Chen K. Crushing analysis and multiobjective crashworthiness optimization of honeycomb-filled single and bitubular polygonal tubes. Mater Des 2011;32(8–9):4449–60.
[23] Bi J, Fang HB, Wang QA, Ren XC. Modeling and optimization of foam-filled thin-walled columns for crashworthiness designs. Finite Elem Analysis Des 2010;46(9):698–709.
[24] Wierzbicki T, Recke L, Abramowicz W, Gholami T, Huang J. Stress profiles in thin-walled prismatic columns subjected to crush loading-II. Bending. Comput Struct 1994;51(6):625–41.
[25] Kim TH, Reid SR. Bending collapse of thin-walled rectangular section columns. Comput Struct 2001;79(20–21):1897–911.
[26] Chen W. Experimental and numerical study on bending collapse of aluminum foam-filled hat profiles. Int J Solids Struct 2001;38(44–45):7919–44.
[27] Zhang ZH, Liu ST, Tang ZL. Design optimization of cross-sectional configuration of rib-reinforced thin-walled beam. Thin Walled Struct 2009;47(8–9):868–78.

[28] Kallina I, Zeidler F, Baumann K, Scheunest D. The offset crash against a deformable barrier, a more realistic frontal impact. In: Proceedings of the 14th international technical conference on enhanced safety of vehicles (ESV). Munich , Germany: Institute for Road Safety Research; 1994. p. 1300–4.
[29] Kecman D. Bending collapse of rectangular and square section tubes. Int J Mech Sci 1983;25(9–10):623–36.
[30] Liu YC, Day ML. Bending collapse of thin-walled beams with channel cross-section. Int J Crashworthiness 2006;11(3):251–62.
[31] Huang X, Lu G. Bending hinge characteristic of thin-walled square tubes. Int J Crashworthiness 2005;10(3):275–85.
[32] Zarei HR, Kroger M. Bending behavior of empty and foam-filled beams: structural optimization. Int J Impact Eng 2008;35:521–9.
[33] Santosa S, Wierzbicki W. Effect of an ultralight metal filler on the bending collapse behavior of thin-walled prismatic columns. Int J Mech Sci 1999;41(8):995–1019.
[34] Santosa S, Banhart J, Wierzbicki T. Experimental and numerical analyses of bending of foam-filled sections. Acta Mech 2001;148(1–4):199–213.
[35] Chen W, Wierzbicki T, Santosa S. Bending collapse of thin-walled beams with ultralight filler: numerical simulation and weight optimization. Acta Mech 2002;153(3–4):183–206.
[36] Guo LW, Yu JL, Li ZB. Experimental studies on the quasi-static bending behavior of double square tubes filled with aluminum foam. Acta Mech 2010;213(3–4):349–58.
[37] Guo LW, Yu JL. Dynamic bending response of double cylindrical tubes with aluminum foam. Int J Impact Eng 2011;38:85–94.
[38] Reyes A, Hopperstad OS, Hanssen AG, Langseth M. Modeling of material failure in foam-based components. Int J Impact Eng 2004;30(7):805–34.
[39] Fang JG, Gao YK, Sun GY, Zhang YT, Li Q. Parametric analysis and multi-objective optimization for functionally graded foam-filled thin-wall tube under lateral impact. Comput Mater Sci 2014;90:265–75.
[40] Hanssen AG, Hopperstad OS, Langseth M, Ilstad H. Validation of constitutive models applicable to aluminium foams. Int J Mech Sci 2002;44(2):359–406.
[41] Chuang CH, Yang RJ, Li G, Mallela K, Pothuraju P. Multidisciplinary design optimization on vehicle tailor rolled blank design. Struct Multidiscip Optim 2008;35(6):551–60.
[42] Sun GY, Xu FX, Li GY, Li Q. Crashing analysis and multiobjective optimization for thin-walled structures with functionally graded thickness. Int J Impact Eng 2014;64:62–74.
[43] Eberhart R, Kennedy J. A new optimizer using particle swarm theory. In: Proceedings of the sixth international symposium on micro machine and human science, Nagoya. Japan: IEEE; 1995. p. 39–43.
[44] Kim HS. New extruded multi-cell aluminum profile for maximum crash energy absorption and weight efficiency. Thin Walled Struct 2002;40(4):311–27.
[45] Zarei HR, Kroger M. Crashworthiness optimization of empty and filled aluminum crash boxes. Int J Crashworthiness 2007;12(3):255–64.
[46] LS-DYNA keyword user's manual: nonlinear dynamic analysis of structures. Version 971. vols. 1-2. California, Livermore Software Technology Corporation; May 2007.
[47] Zhao D, Xue DY. A multi-surrogate approximation method for metamodeling. Eng Comput 2011;27(2):139–53.
[48] Fang JG, Gao YK, Sun GY, Li Q. Multiobjective reliability-based optimization for design of a vehicle door. Finite Elem Analysis Des 2013;67:13–21.
[49] Gutmann HM. A radial basis function method for global optimization. J Glob Optim 2001;19(3):201–27.
[50] Olsson A, Sandberg G, Dahlblom O. On latin hypercube sampling for structural reliability analysis. Struct Saf 2003;25(1):47–68.
[51] Song XG, Sun GY, Li GY, Gao WZ, Li Q. Crashworthiness optimization of foam-filled tapered thin-walled structure using multiple surrogate models. Struct Multidiscip Optim 2013;47(2):211–31.
[52] Raquel CR, Naval PC. An effective use of crowding distance in multiobjective particle swarm optimization. In: Proceedings of the 7th annual conference on genetic and evolutionary computation. New York, USA: ACM; 2005. p. 257–64.

View publication stats